Intersystem Crossing and Characterization of Dark States in the Pyrimidine Nucleobases Uracil, Thymine, and 1-Methylthymine†

Mihajlo Etinski,‡ Timo Fleig,‡,§ and Christel M. Marian*,‡

Institute of Theoretical and Computational Chemistry, Heinrich Heine University Düsseldorf, Düsseldorf, Germany

Received: March 31, 2009; Revised Manuscript Received: July 10, 2009

The ground and low-lying excited states of the pyrimidine nucleo bases uracil, thymine, and 1-methylthymine have been characterized using ab initio coupled-cluster with approximate doubles (CC2) and a combination of density functional theory (DFT) and semiempirical multireference configuration interaction (MRCI) methods. Intersystem crossing rate constants have been determined perturbationally by employing a nonempirical one-center mean-field approximation to the Breit−Pauli spin−orbit operator for the computation of electronic coupling matrix elements. Our results clearly indicate that the $S_2(^1\pi\rightarrow\pi^*)$ ⇝ $T_2(^3n\rightarrow\pi^*)$ process cannot compete with the subpicosecond decay of the S_2 population due to spin-allowed nonradiative transitions, whereas the $T_1(^3\pi\rightarrow\pi^*)$ state is populated from the intermediate $S_1(^1n\rightarrow\pi^*)$ state on a subnanosecond time scale. Hence, it is very unlikely that the $S_1(^1n\rightarrow\pi^*)$ state corresponds to the long-lived dark state observed in the gas phase.

Introduction

The most significant photophysical property of the pyrimidine nucleo bases is their ultrafast decay to the ground state after UV irradiation,[1] both in the gas phase[2−6] and in solution.[7−11] It is agreed nowadays that this behavior is a consequence of energetically low-lying conical intersections and the concomitant strong nonadiabatic coupling between the primarily excited $^1\pi \rightarrow \pi^*$ state, the lowest $^1n \rightarrow \pi^*$ state, and the electronic ground state.[10,12−21]

Despite the ultrafast relaxation of the majority of the nucleobases, photochemical dimerization of the pyrimidine bases[22,23] is an abundant photolesion of the DNA after UV irradiation. For a long time, the mechanisms of the dimerization reactions, i.e., the formation of a cyclobutane dimer, (6−4) photoproduct, or the spore photoproduct, were believed to proceed via a transient triplet state.[24] Recently, indications were presented, however, that the thymine dimerization is an ultrafast process.[25−27] This finding does not exclude the participation of a triplet mechanism. Rather, quantum chemical studies[28−31] were able to show that two mechanisms exist: A concerted (one-step) cyclobutane formation on an excited singlet potential energy hypersurface (PEH) and a two-step ring-closure on the lowest triplet PEH.

Gas-phase experiments often can give detailed information about energy levels and relaxation dynamics. Vapor spectra of some pyrimidine bases were recorded long ago,[32] but the absorption bands were found to be broad and structureless. Vibrationally resolved electronic excitation of gaseous thymine using electron energy loss (EEL) techniques was reported,[33] revealing the absorption maxima of various singlet transitions. Furthermore, a band in the low energy regime was attributed to the lowest triplet state (T_1). However, uracil and thymine do not have sharp resonance-enhanced multiphoton ionization (REMPI) spectra.[34] Femtosecond time-resolved experiments in supersonic jets revealed that the decay signal from the first bright state of uracil and thymine exhibits a multiexponential behavior that represents different relaxation channels.[2,3,5] On the basis of quantum molecular dynamics simulations Hudock et al.[19] attributed the femtosecond component to the relaxation from the Franck−Condon (FC) region to the minimum of the $^1\pi \rightarrow \pi^*$ state. Their calculations suggest that the ionization potential increases substantially along this relaxation pathway, thus explaining the lack of REMPI spectra. The picosecond component was assigned to the process of crossing the barrier connecting the minimum of the $^1\pi \rightarrow \pi^*$ potential energy surface to the conical intersection between the $^1\pi \rightarrow \pi^*$ (S_2) and $^1n \rightarrow \pi^*$ (S_1) states. Other authors presented different interpretations of the multiexponential decay process. Lan et al.[21] using semiempirical surface-hopping molecular dynamics propose a two-step relaxation mechanism for uracil and thymine with a $^1\pi \rightarrow \pi^*$ (S2) ⇝ $^1n \rightarrow \pi^*$ (S_1) deexcitation on the femtosecond time scale and a subsequent internal conversion (IC) of the S_1 state to the electronic ground state on the picosecond time scale. In addition, these authors find a small contribution from trajectories of a direct decay of the $^1\pi \rightarrow \pi^*$ state to the ground state. Conical intersections between the S_2/S_1, the S_2/S_0, and the S_1/S_0 states of uracil and thymine were also located in numerous steady-state quantum chemical investigations.[10,12,14−18,35]

Interestingly, nanosecond time-resolved experiments in the gas phase found indications for a long-lived dark state in methylated uracils and thymines.[36−38] Kong and co-workers[36,37] found its lifetime to vary from a few tens to hundreds of nanoseconds depending on the degree of methylation and the energy of the initial excitation. They showed that methylation stabilizes the dark state whereas it is quenched by microhydration. In contrast, recently Busker et al.[38] observed the dark state also in microhydrated 1-methylthymine. Both groups characterized the dark state as $^1n \rightarrow \pi^*$.

In the condensed phase, Hare et al.,[11,39] using femtosecond transient absorption techniques, found two decay channels from the primarily excited $^1\pi \rightarrow \pi^*$ state, i.e., direct IC to the ground

† Part of the "Walter Thiel Festschrift".

* Corresponding author. E-mail: Christel.Marian@uni-duesseldorf.de.
‡ HHU Düsseldorf.
§ Current address: IRSAMC, Université Paul Sabatier, Toulouse, France.

10.1021/jp902944a CCC: $40.75
Published on Web 08/11/2009

state and decay to the $^1n \rightarrow \pi^*$ state, which was also proposed as a gateway for the triplet-state population. In a later study, Hare et al.[40] used time-resolved infrared (TRIR) spectroscopy in the excited state and comparison with a simulated S_0-T_1 spectrum to identify the long-lived dark state. They concluded that the triplet state is formed within 10 ps after excitation and that the vibrationally relaxed $^1n \rightarrow \pi^*$ state is not the precursor for the triplet formation. The triplet quantum yield φ_T ranges from 0.02 in water up to 0.54 in ethylacetate for 1-cyclohexyluracil.[39] The general trend is that φ_T increases going from polar protic solvents to nonpolar solvents.

Serrano-Andrés and co-workers performed quantum chemical calculations on the isolated pyrimidine bases to explain how the lowest triplet state $^3\pi \rightarrow \pi^*$ is formed in uracil[41] and thymine.[42] In essence, they propose three pathways for populating the $^3\pi \rightarrow \pi^*$ state from the initially excited $^1\pi \rightarrow \pi^*$ state. The first one proceeds via the intermediate $^3n \rightarrow \pi^*$ state whereas the second is a direct intersystem transition $^1\pi \rightarrow \pi^* \rightsquigarrow {}^3\pi \rightarrow \pi^*$ at the intersection of the latter potential energy surfaces. The third mechanism includes IC to the $^1n \rightarrow \pi^*$ state followed by intersystem crossing (ISC) to the $^3\pi \rightarrow \pi^*$ state. In all cases electronic spin−orbit coupling matrix elements (SOMEs) were found to be sizable. It is well-known, however, that large electronic spin−orbit coupling does not automatically bring about high ISC rates, because the latter depend crucially on the vibrational overlaps of the initial and final states.[43]

Understanding the nature of the dark state is an important issue because it can reveal how various photoproducts are formed. The purpose of the present study is to characterize the experimentally observed long-lived dark state of uracil, thymine and 1-methylthymine.[27,36−40] The paper is organized as follows: In the next section we summarize computational methods and basis sets that were used for our calculations. In the subsequent section we present ground- and excited-state structures, vibrational frequencies, and vertical and adiabatic electronic excitation energies. Furthermore, various paths for ISC are investigated and related rates are determined. Finally, we discuss the results and draw conclusions from our study.

Theoretical Methods and Computational Details

We employed the following electronic structure methods: coupled-cluster with approximate treatment of doubles (CC2), density functional theory (DFT) and the combined density functional theory/multireference configuration interaction (DFT/MRCI) approach. The CC2 method[44] is an approximation to the coupled-cluster singles and doubles (CCSD) method where the singles equations are retained in the original form and the doubles equations are truncated to first order in the fluctuating potential. We used the resolution-of-identity (RI)[45] CC2 implementation in TURBOMOLE[46] for the ground state[47] and in combination with linear response theory for excited-state optimizations,[48] vertical excitation energies and the calculation of properties.[49] We utilized DFT, unrestricted DFT (UDFT), and time-dependent DFT (TDDFT)[50] with the B3-LYP[51] functional implementation of TURBOMOLE[52] for ground-state and excited-state optimizations. The SNF[53] program was employed for numerical calculations of vibrational frequencies in harmonic approximation. In the DFT/MRCI method[54] dynamic electronic correlations are taken mainly into account by DFT. Static electronic correlations are obtained from multireference configuration interaction expansions employing a one-particle basis of BH-LYP Kohn−Sham molecular orbitals.[55,56] Double-counting of dynamic electron correlation is avoided by extensive configuration selection. In all electronic structure calculations only valence electrons were correlated.

We used Dunning's[57,58] correlation-consistent basis sets cc-pVDZ (C, N, O, 9s4p1d/3s2p1d; H, 4s1p/2s1p) and aug-cc-pVTZ (C, N, O, 11s6p3d2f/5s4p3d2f; H, 6s3p2d/4s3p2d) and the standard TZVP (C, N, O, 10s6p1d/4s3p1d; H, 5s1p/3s1p) basis sets from the TURBOMOLE library.[59] Auxiliary basis sets for the RI approximation of the two-electron integrals in the CC2 and MRCI treatments were taken from the TURBOMOLE library.[60,61]

SOMEs were evaluated for DFT/MRCI electronic wave functions using SPOCK.[62] Herein a one-center mean-field approximation to the Breit−Pauli Hamiltonian is employed.[63,64] This approximation typically reproduces results within 5% of the full treatment.[65,66] ISC rates were calculated using the methods described in detail elsewhere.[67,68] If not stated otherwise, we made use of the Condon approximation employing a constant electronic SOME evaluated at the minimum of the initial state multiplied by FC factors. For intercombination transitions of the type $^1\pi \rightarrow \pi^* \rightsquigarrow {}^3\pi \rightarrow \pi^*$, earlier work in our laboratory[67,68] had shown that it is necessary to go beyond the Condon approximation. In these cases, a Herzberg−Teller (HT) like expansion up to first order in the normal coordinates was carried out. To obtain ISC rates, matrix elements were calculated between the $\upsilon = 0$ vibrational wave function of the initial electronic state and vibrational wave functions of the final electronic state with energies in a small interval of width 2η. In test calculations, values of η ranged from 0.001 to 10 cm^{-1}. For the final ISC rates, interval widths between 0.001 and 0.01 cm^{-1} were chosen.

Results and Discussion

Ground-State Geometries and Vertical Excitation Energies. The ground-state equilibrium structures of uracil, thymine, and 1-methylthymine were optimized using the B3-LYP/DFT/TZVP and RI-CC2/cc-pVDZ levels of computation. Bond lengths obtained with these two methods are presented in Figures 1−3. As a general trend, the B3-LYP/DFT/TZVP equilibrium bond distances are somewhat shorter than the corresponding RI-CC2/cc-pVDZ values. Comparison of our RI-CC2/cc-pVDZ optimized geometries for uracil and thymine with the benchmark RI-CC2 calculations by Fleig et al.[69] reveals that improvement of the basis set leads to a slight bond contraction. The best values in that work (aug-cc-pVTZ/CC2 for thymine and aug-cc-pVQZ/CC2 for uracil) are essentially exact in comparison with experiment.[70] It should be kept in mind, however, that the X-ray structural parameters for uracil[70] were determined in the crystalline state that contains hydrogen-bonded uracil dimers. A more appropriate comparison with experimental values is possible for thymine where gas-phase electron diffraction and microwave data are available.[71] The experimentally derived bond lengths are displayed in Figure 2 in square brackets. Comparison with our B3-LYP/DFT/TZVP optimized values (given in parentheses) and RI-CC2/cc-pVDZ parameters (plain numbers) yields overall good agreement for the single bonds and shows that the DFT results for the lengths of the double bonds are closer to experiment, at least for the electronic ground state.

Computed vibrational spectra associated with the electronic ground state and available gas-phase spectral data are given in Tables S1, S7, and S11 of the Supporting Information. With the exception of a peak at 1897 cm^{-1} and a shoulder at 1356 cm^{-1} all peaks in the experimental gas-phase spectrum of uracil[72] in the mid-infrared region can be assigned unambiguously. Also for the thymine bands of very strong, strong, and medium intensity, a one-to-one correspondence between experiment[72] and theory can be established. In the wavenumber region below

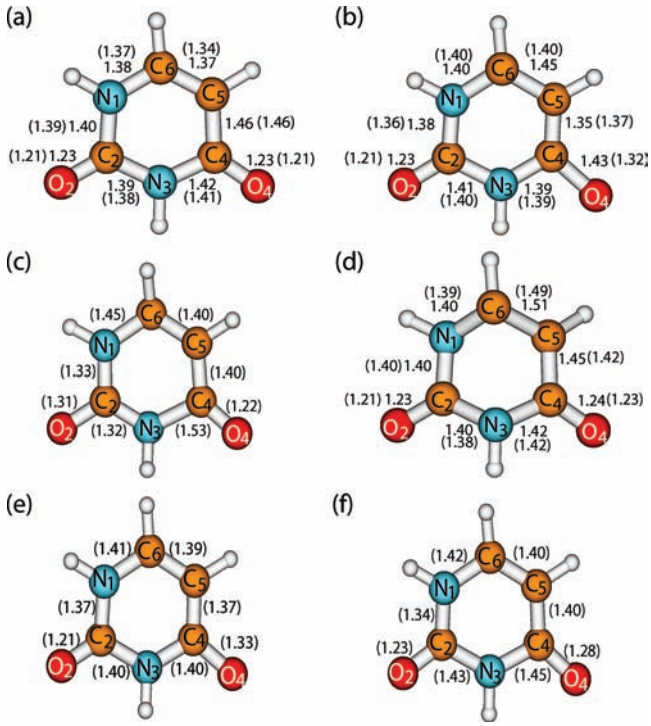

Figure 1. Stationary points of ground and excited-state PEHs of uracil, optimized at the RI-CC2/cc-pVDZ (B3-LYP/DFT/TZVP) levels: (a) ground-state minimum; (b) $S_1(n\rightarrow\pi^*)$ minimum; (c) saddle point structure of $S_2(\pi\rightarrow\pi^*)$ with one imaginary frequency; (d) $T_1(\pi\rightarrow\pi^*)$ minimum; (e) $T_2(n\rightarrow\pi^*)$ minimum; (f) $T_3(\pi\rightarrow\pi^*)$ minimum. All bond lengths are in Å.

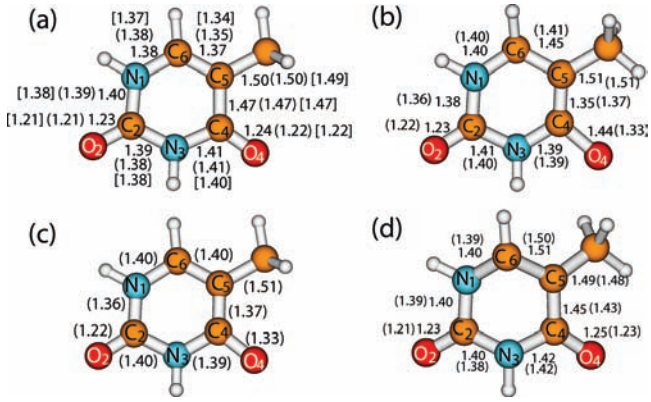

Figure 2. Stationary points of ground and excited-state PEHs of thymine, optimized at the RI-CC2/cc-pVDZ (B3-LYP/DFT/TZVP) levels: (a) ground-state minimum; (b) $S_1(n\rightarrow\pi^*)$ minimum with 60° rotated methyl group (it represents the global minimum at the RI-CC2/cc-pVDZ level whereas it is a local minimum at the B3-LYP/UDFT/TZVP level); (c) S_1-state global minimum structure obtained at the B3-LYP/UDFT/TZVP level; (d) T_1 $(\pi\rightarrow\pi^*)$ minimum. Experimental bond lengths[71] are displayed in square brackets. All bond lengths are in Å.

1000 cm^{-1}, however, calculated and measured intensities do not match well in several cases, most certainly because the harmonic approximation is too crude for soft modes. For more details see the Supporting Information.

Vertical electronic excitation energies of the lowest excited singlet and triplet states are compiled in Table 1. The S_1 state exhibits $n \rightarrow \pi^*$ character in the FC region of all three compounds whereas the first optically bright band originates from a transition to the $S_2(\pi\rightarrow\pi^*)$ state. Three triplet states are found energetically below or at least close to the S_2 state. To give a comprehensive overview over the excitation energies obtained with various quantum chemical methods and basis sets is far beyond the purpose of the present work. Suffice it to say that the orders of singlet states are identical in most of the recent theoretical works,[10,12,14−19,21,35,38,41,69,73−79] whereas the actual energy gaps vary considerably. For a comparison with our results in Table 1 we picked only a few studies that used either the same methods or basis sets.

Comparing the spectra of the three compounds for a fixed combination of method and basis set, one sees that the excitation energies of the $n \rightarrow \pi^*$ states are nearly constant whereas a marked stabilization is observed for the $S_2(\pi\rightarrow\pi^*)$ state when proceeding from uracil over thymine (=5-methyluracil) to 1-methylthymine (=1,5-dimethyluracil). A similar but less pronounced effect is found for the T_1 state. The methylation effect can be explained by the differential impact of the electron-donating methyl group that affects π orbitals (ring, delocalized) more strongly than an *n* orbital (which is much more localized). The magnitude of the effect in substituted uracils is, indeed, remarkable. Ongoing theoretical investigations on 1-methyluracil, an isomer of thymine, and 1,3-dimethyluracil, an isomer of 1-methylthymine, show that these species exhibit different electronic spectra and that the observed shifts are not artifacts of a basis set superposition error.[80]

Augmentation of the basis set at a fixed nuclear geometry lowers the CC2 excitation energies. Again, the energies of the S_2 states take the largest advantage from the improvement of the basis set. This is in line with an observation relating to CASSCF and CASPT2 excitation energies of the nucleobases[16,41,74] from which it is well-known that dynamic electron correlation effects are significantly larger for the $^1\pi \rightarrow \pi^*$ excitations than for $^1n \rightarrow \pi^*$ or triplet states. On the other hand, changing the nuclear geometry from the RI-CC2/cc-pVDZ to the B3-LYP/DFT/TZVP optimized structure while keeping the correlation method and basis set constant, leads to a nearly uniform blue shift of the $n \rightarrow \pi^*$ and $\pi \rightarrow \pi^*$ excitation energies by 0.12−0.14 eV. The geometry effect can be rationalized on the basis of bond length changes. In both, the $n \rightarrow \pi^*$ and the $\pi \rightarrow \pi^*$ states, the C_5-C_6 and the C−O double bonds are markedly extended at equilibrium (see next paragraph). The CC2- and MP2-optimized geometry parameters thus yield lower excitation energies with respect to the electronic ground state. DFT/MRCI gives larger gaps between the first two excited singlet states than the CC2 method. Also, it generally gives lower triplet-state excitation energies. Only a few experimental gas-phase data are available for comparison. It appears that the observed band maxima of the $S_2 \leftarrow S_0$ transitions in uracil and thymine are located at longer wavelengths than the vertical excitation wavelengths in the calculations.

Excited-State Properties. For uracil, we optimized the nuclear arrangements of the first two excited singlet states and the three lowest-lying triplet states. In the case of the methylated compounds, we searched only for the minimum structures of the respective S_1 and T_1 states. Bond lengths of the optimized excited-state structures are displayed in Figures 1−3. Adiabatic excitation energies are collected in Table 2 together with results of previous theoretical work.[41,42,81] Nuclear coordinates and harmonic vibrational frequencies of all optimized structures are provided in the Supporting Information.

The most outstanding characteristic of the nearly planar $S_1(n\rightarrow\pi^*)$ geometry is that the C_4-O_4 bond is significantly elongated compared to the C_2-O_2 bond by 0.20 Å (RI-CC2) or 0.11 Å (DFT). Since there are no experimental nuclear geometry data available for the S_1 state, it can presently not be decided which C_4-O_4 bond length is more realistic. Ab initio

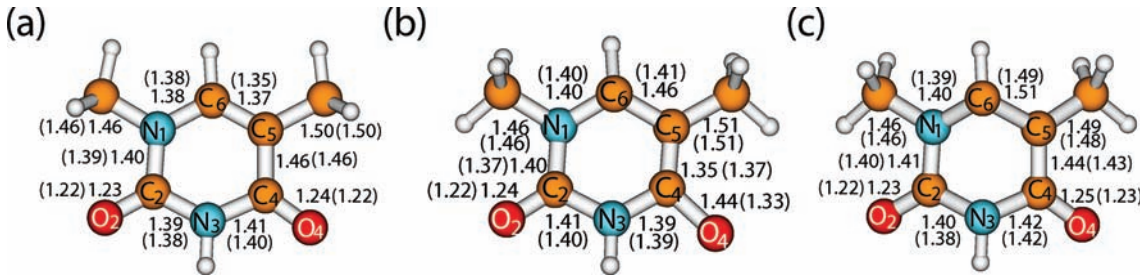

Figure 3. Minimum nuclear arrangements of 1-methylthymine optimized at the RI-CC2/cc-pVDZ (B3-LYP/DFT/TZVP) levels: (a) ground-state minimum; (b) $S_1(n\rightarrow\pi^*)$ minimum; (c) $T_1(\pi\rightarrow\pi^*)$ minimum. All bond lengths are in Å.

CASSCF[15] and MRCI singles[17] results using comparable basis sets as well as the semiempirical OM2-MRCI values[21] are much closer to the TDDFT values. RI-CC2 yields a minimum structure with the methyl group rotated by 60° with respect to the ground state (Figure 2b). This nuclear arrangement represents also a local minimum on the TDDFT PEH, the global minimum of which is found for the same orientation of the methyl group as in the ground state (Figure 2c). The subsequent DFT/MRCI calculations reverse the energetic order of these two minima. Thus, the structure displayed in Figure 2b is considered to be the global minimum at the DFT/MRCI level, too. In 1-methylthymine, both methyl groups are rotated by 60° with respect to the ground-state structure. Vibrational spectra in harmonic approximation associated with the S_1 states are given in Tables S2, S8, and S12 of the Supporting Information. In line with the larger geometry change, the energy release upon relaxation of the nuclear arrangement in the S_1 state is larger at the RI-CC2 level. Despite their considerably higher vertical absorption energies, the adiabatic excitation energies of the S_1 states of uracil, thymine, and 1-methylthymine are lower at the RI-CC2 level than the corresponding DFT/MRCI values (Table 2).

At the RI-CC2/cc-pVDZ level of calculation, stationary points for the S_2 states of the three compounds could not be located. When the planarity constraint is lifted, continued root flipping between the lowest $^1\pi\rightarrow\pi^*$ and $^1n\rightarrow\pi^*$ states occurs after a few steps of initial energy relaxation, indicating a nearby intersection of the corresponding PEHs. A similar behavior was reported by other authors.[15] The existence of a true S_2 equilibrium structure is discussed controversially in the literature.[15−17,19,21] It appears that the barrier separating the S_2 minimum from the conical intersection region diminishes upon inclusion of dynamic electron correlation. At the B3-LYP/TDDFT/TZVP level we obtained a first-order saddle point for the S_2 state of uracil. The imaginary frequency (ν = i59 cm^{-1}) is associated with a puckering mode that exhibits the largest amplitude for a pyramidalization at the N_3 center. The saddle point exhibits an almost planar geometry with the H atom attached to C_6 pointing out of plane. Compared to the ground-state geometry, the most significant bond length changes occur in the ring bonds (see Figure 1). In addition, the C_2-O_2 bond is markedly elongated, in good agreement with recent CASSCF results by Perun et al.[15] and MRCI singles results by Yoshikawa and Matsika,[17] but at variance with the CASSCF and CASPT2 optimized structures by Hudock et al.[19] Note that a single-point DFT/MRCI calculation, carried out at the saddle-point structure, yields a substantially higher excitation energy of the S_2 state (5.25 eV) than at the T_1 minimum geometry (5.01 eV).

The T_1 state results from a HOMO → LUMO excitation and exhibits $\pi\rightarrow\pi^*$ character. The geometry is slightly butterfly shaped where the CC2 optimized structure is more folded compared to the UDFT geometry. The most significant bond length change with respect to the ground-state geometry parameters occurs for the C_5-C_6 bond that is elongated by about 0.15 Å. At the B3-LYP/UDFT/TZVP and CC2/cc-pVDZ levels, the minimum is found for a structure with the methyl group rotated by 60°. In 1-methylthymine, both methyl groups are rotated with respect to the ground-state structure but have the same orientation as in the S_1 state. The adiabatic excitation energies, computed at the DFT/MRCI level, are somewhat lower than those obtained at the RI-CC2 level (see Table 2). Harmonic frequencies are given in Tables S4, S10, and S13 of the Supporting Information.

In principle, TRIR spectroscopy in the excited state can be used to identify the long-lived dark state. Such measurements were conducted by Hare et al.[40] for thymine in argon-purged deuterated acetonitrile. They monitored in particular the shifts in the C═O stretching frequencies upon electronic excitation and concluded that the transient species is the T_1 state. However, as will be outlined in more detail in the Supporting Information, the assignment of the dark state based on the shifts of the C═O stretching frequencies is not conclusive, since the simulated S_0-T_1 and S_0-S_1 difference spectra look very similar in that wavenumber region (Figure S1 of the Supporting Information). Characteristic of the S_0-T_1 difference spectrum are a peak near 1500 cm^{-1} that results from a combination of the $C_4{=}C_5$ stretching and the N_1H wagging motions and a peak near 1350 cm^{-1} that arises from a ring deformation vibration. Particularly the S_0-T_1 spectrum computed at the RI-CC2 level reproduces all experimental features excellently whereas significant deviations are noticed for the low-frequency region of the simulated S_0-S_1 spectrum. We are therefore confident that the TRIR spectrum observed by Hare et al.[40] stems from the transient T_1 state of thymine and not from the S_1 state.

The T_2 state has $n\rightarrow\pi^*$ character. As may be expected, its minimum geometry parameters are nearly indistinguishable from those of the corresponding singlet state (S_1) and the singlet−triplet splitting of the $n\rightarrow\pi^*$ states is rather small. The T_3 state originates from a single excitation of an electron from a π orbital that is located mainly at the two oxygen atoms and the intermediate N_3 atom to the LUMO. Its minimum is located energetically below the lowest point of the S_2 state and is thus of interest for ISC processes. Also this state exhibits a planar minimum geometry.

Intersystem Crossings. For uracil, transition rates for three different nonradiative singlet−triplet pathways were calculated:

(a) $S_1(^1n\rightarrow\pi^*) \rightsquigarrow T_1(^3\pi\rightarrow\pi^*)$

(b) $S_2(^1\pi\rightarrow\pi^*) \rightsquigarrow T_2(^3n\rightarrow\pi^*)$

(c) $S_2(^1\pi\rightarrow\pi^*) \rightsquigarrow T_3(^3\pi\rightarrow\pi^*)$

For thymine and 1-methylthymine only pathway (a) was taken into consideration. Our methods do not allow us to compute ISC rates for vibrationally hot states. The dependence of the ISC dynamics on the excess energy in the S_1 state, as observed by Hare et al.[39] for 1-cyclohexyluracil, was therefore not investigated in the present work.

TABLE 1: Vertical Excitation Spectrum of Uracil, Thymine, and 1-Methylthymine at the Ground-State Geometry (eV)[a]

state	CC2/cc-pVDZ//CC2/cc-pVDZ	CC2/aug-cc-pVTZ//CC2/cc-pVDZ	CC2/aug-cc-pVTZ//B3-LYP/TZVP	DFT/MRCI/TZVP//B3-LYP/TZVP	CC2/TZVP//MP2/6-31G★[b]	DFT/MRCI/TZVP//MP2/6-31G★[c]	CC2/aug-cc-pVQZ//CC2/aug-cc-pVQZ[d]	experiment
				Uracil				
$S_1(n\rightarrow\pi^*)$	4.91	4.78	4.91	4.67	4.91	4.41	4.80	
$S_2(\pi\rightarrow\pi^*)$	5.54	5.25	5.38	5.56	5.52	5.33	5.35	5.08[e]
$T_1(\pi\rightarrow\pi^*)$	3.90	3.84	3.97	3.78			3.95	3.65[f]
$T_2(n\rightarrow\pi^*)$	4.66	4.58	4.70	4.46			4.60	
$T_3(\pi\rightarrow\pi^*)$	5.44		5.50	5.16			5.42	
				Thymine				
$S_1(n\rightarrow\pi^*)$	4.96	4.80	4.94	4.59	4.94	4.48	4.82	
$S_2(\pi\rightarrow\pi^*)$	5.44	5.12	5.25	5.26	5.39	5.18	5.20	4.80,[g] 4.95[h]
$T_1(\pi\rightarrow\pi^*)$	3.82	3.72	3.86	3.54			3.82	3.60[h]
$T_2(n\rightarrow\pi^*)$	4.70	4.59	4.73	4.37			4.61	
$T_3(\pi\rightarrow\pi^*)$	5.43			4.98			5.39	
				1-Methylthymine				
$S_1(n\rightarrow\pi^*)$	4.96	4.78[i]	4.92	4.59				
$S_2(\pi\rightarrow\pi^*)$	5.23	4.88[i]	5.01	5.10				
$T_1(\pi\rightarrow\pi^*)$	3.76	3.64[i]	3.78	3.46				
$T_2(n\rightarrow\pi^*)$	4.72	4.59[i]	4.72	4.38				
$T_3(\pi\rightarrow\pi^*)$	5.37	5.24[i]		4.91				

[a] Method used for calculation of vertical spectrum//method used for geometry optimization of the ground state. [b] Schreiber et al.[78] [c] Silva-Junior et al.[79] [d] Fleig et al.[69] [e] Vapor spectrum, Clark et al.[32] [f] Electron energy loss specroscopy, Abouaf et al., cited as private communication in ref 81. [g] Gas-phase absorption of 1,3-methyluracil, Clark et al.[32] [h] Electron energy loss specroscopy, Abouaf et al.[33] [i] Busker et al.[38]

In the Condon approximation, electronic SOMEs for a pair of states are required only at a single geometry $\mathbf{q_0}$, about which the Taylor series of the interaction is expanded. Typically, the equilibrium geometry of the initial state is chosen as offset for the Taylor expansion. We made this choice for process a whereas in cases b and c the saddle point of the primarily excited $^1\pi\rightarrow\pi^*$ state was used due to the absence of a true minimum geometry. Furthermore, for computing the FC and HT matrix elements of the zero-point vibrational level of the S_2 state the harmonic frequency of the imaginary mode was set to $+100$ cm^{-1}.

In Table 3, SOMEs computed at the respective S_1 minima are collected. They are large, agreeing with recent theoretical work of Serrano-Pérez et al.[42] but contradicting the conclusions drawn by Hare et al.[39] who predicted that the relaxed $^1n\rightarrow\pi^*$ state has negligible spin−orbit coupling with the $^3\pi\rightarrow\pi^*$ state. The Cartesian components of the electronic SOMEs depend on the molecular orientation in a space-fixed coordinate system. In the Condon approximation it is sufficient to use the sum over the squared electronic matrix elements of the components (given as additional entries in Table 3) for randomly oriented molecules in the gas phase or in solution. These sums vary only slightly when proceeding from uracil to thymine and 1-methylthymine.

Calculated $S_1 \rightsquigarrow T_1$ ISC rates are shown in Table 4. Although the electronic coupling strengths are nearly identical at the RI-CC2 and TDDFT optimized geometries, the resulting rates differ by a factor of about 25 for uracil and by up to 2 orders of magnitude for thymine. At first sight, this is counterintuitive since the S_1/T_1 energy gaps are smaller in the CC2 case. For the smallest of the three systems, uracil, therefore, a series of calculations was carried out, testing—among other parameters—the dependence of the ISC rates on the electronic energy difference between the pair of coupling states. Interestingly, the computed ISC rate increases dramatically (by nearly 3 orders of magnitude) when the energy gap is varied from 4000 to 8000 cm^{-1} where a maximum evolves (see Table S17, Supporting Information, for further details). This strange behavior results from a trade-off between the vibrational density of states and the overlap of the vibrational wave functions. Using the DFT-optimized potentials shifted vertically to match the adiabatic energy difference of the RI-CC2 method (5150 cm^{-1}) yields an ISC rate of 1.4×10^{11} s^{-1}, somewhat smaller than the value (2.3×10^{11} s^{-1}) computed with the DFT/MRCI method but in the same ballpark. We interpret the much lower ISC rate (0.9×10^{10} s^{-1}) calculated for the RI-CC2 potentials as being caused mainly by a larger coordinate displacement and concomitant smaller vibrational overlap. Nevertheless, even with these uncertainties the lifetime of the S_1 state with respect to this ISC process (5−100 ps) is significantly shorter than the lifetime of the dark state in the gas-phase experiments, ranging from about 20 to 200 ns depending on the methylation and the laser excitation energy.[36−38] The calculated $S_1 \rightsquigarrow T_1$ ISC rates of thymine and 1-methylthymine are somewhat smaller than those of the corresponding process in uracil, but the order of magnitude is conserved.

To gain further insight, we calculated a linearly interpolated path between the UDFT-optimized T_1 geometry (RC = 0) of uracil and the TDDFT-optimized S_1 minimum (RC = 1.0) and extended this path on both sides. This energy profile (Figure 4) shows a crossing between the shallow PEH of the primarily excited $S_2(\pi\rightarrow\pi^*)$ state and the $S_1(n\rightarrow\pi^*)$ state in the neighborhood of the T_1 (and presumably also the S_2) minimum nuclear geometry, in accord with the findings of previous theoretical work on uracil and thymine where a conical intersection is

TABLE 2: Adiabatic Excitation Energies of Uracil, Thymine, and 1-Methylthymine (eV)[a]

state	CC2/cc-pVDZ// CC2/cc-pVDZ	CC2/aug-cc-pVTZ// CC2/cc-pVDZ	DFT/MRCI/TZVP// B3-LYP/TZVP	B3-LYP/6-311++G(3df,2p)// B3-LYP/6-311++G(3df,2p)[b]	CASPT2/ANO-S// CASSCF(14,10)/ANO-S[c]
			Uracil		
$S_1(n\rightarrow\pi^*)$	3.88	3.74	3.96		4.03
$S_2(\pi\rightarrow\pi^*)$			(5.01)[d]		4.48
$T_1(\pi\rightarrow\pi^*)$	3.24	3.31	3.13	3.02	3.15
$T_2(n\rightarrow\pi^*)$			3.84		3.91
$T_3(\pi\rightarrow\pi^*)$			4.58		
			Thymine		
$S_1(n\rightarrow\pi^*)$	3.93	3.73	4.02		4.05
$T_1(\pi\rightarrow\pi^*)$	3.10	3.16	2.96	2.84	2.87
			1-Methylthymine		
$S_1(n\rightarrow\pi^*)$	3.89	3.73	4.03		
$T_1(\pi\rightarrow\pi^*)$	3.06	3.11	2.94		

[a] Method used for calculation of adiabatic energies//method used for geometry optimization of state. [b] Reference 81. [c] References 41 and 42. S_2 minimum of uracil was optimized at the CASPT2 level. [d] TDDFT saddle point; adiabatic energy at the T_1 minimum is displayed.

TABLE 3: Spin−Orbit Matrix Elements $\langle S_1|\hat{H}_{SO}|T_1\rangle$ (cm^{-1}) Calculated at the S_1-State Geometry[a]

component	DFT/MRCI/cc-pVDZ// RI-CC2/cc-pVDZ	DFT/MRCI/aug-cc-pVTZ// RI-CC2/cc-pVDZ	DFT/MRCI/TZVP// TDDFT B3-LYP/TZVP
		Uracil	
$\hat{H}_{SO,x}$	38.95	36.96	7.70
$\hat{H}_{SO,y}$	29.37	32.74	46.25
$\hat{H}_{SO,z}$	−3.39	4.71	−0.04
sum of squares	2391	2460	2198
		Thymine	
$\hat{H}_{SO,x}$	42.46	44.00	44.13
$\hat{H}_{SO,y}$	−20.59	−21.49	10.40
$\hat{H}_{SO,z}$	9.59	9.73	−0.62
sum of squares	2319	2493	2056
		1-Methylthymine	
$\hat{H}_{SO,x}$	−35.78	−36.96	44.75
$\hat{H}_{SO,y}$	−31.65	−32.73	−10.10
$\hat{H}_{SO,z}$	−4.68	4.71	−0.02
sum of squares	2304	2460	2110

[a] Method used for spin−orbit calculation//method used for geometry optimization of state.

TABLE 4: Calculated Rate Constants k_{ISC} (s^{-1}) for the ($S_1 \rightsquigarrow T_1$) ISC Channels in Uracil, Thymine, and 1-Methylthymine[a]

method[b]	ΔE^{ad}	k_{ISC}
Uracil		
RI-CC2/cc-pVTZ//RI-CC2/cc-pVTZ[c]	5150	0.93×10^{10}
DFT/MRCI/TZVP//DFT B3-LYP/TZVP[d]	6704	0.23×10^{12}
Thymine		
RI-CC2/cc-pVDZ//RI-CC2/cc-pVDZ[c]	6652	0.13×10^{10}
DFT/MRCI/TZVP//DFT B3-LYP/TZVP[e]	8426	0.11×10^{12}
1-Methylthymine		
RI-CC2/cc-pVDZ//RI-CC2/cc-pVDZ[e]	6724	0.49×10^{10}

[a] ΔE^{ad} (cm^{-1}) denotes the adiabatic electronic energy difference. [b] Method used for energy calculation//method used for geometry optimization. [c] Interval width of $\eta = 0.01$ cm^{-1} used. All vibrational modes were employed and 5 quanta per mode were allowed. DFT/MRCI/cc-pVDZ wave functions were employed for computing the SOMEs. [d] Interval width of $\eta = 0.01$ cm^{-1} used. All vibrational modes were employed and an unlimited number of quanta per mode were allowed. [e] Interval width of $\eta = 0.001$ cm^{-1} used. All vibrational modes were employed and 3 quanta per mode were allowed.

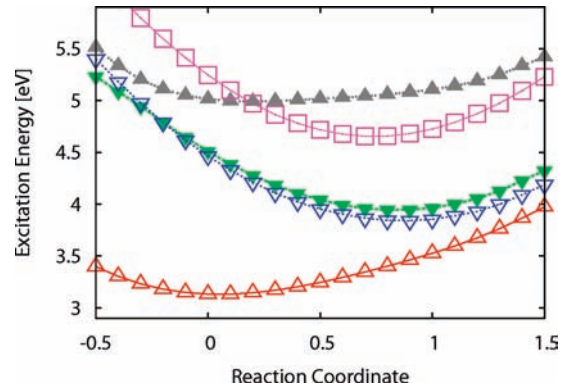

Figure 4. DFT/MRCI/TZVP single-point calculations along a linearly interpolated path between the UDFT-optimized T_1 geometry (RC = 0) of uracil and the TDDFT-optimized S_1 minimum (RC = 1.0) and extended on both sides. $T_1(\pi\rightarrow\pi^*)$: upright open triangles. $T_2(n\rightarrow\pi^*)$: upside down open triangles. $S_1(n\rightarrow\pi^*)$: upside down filled triangles. $T_3(\pi\rightarrow\pi^*)$: open squares. $S_2(\pi\rightarrow\pi^*)$: upright filled triangles.

reported in this area of the coordinate space.[10,12,14−19,21,35] In addition, we find an intersection between the $S_2(\pi\rightarrow\pi^*)$ and $T_3(\pi\rightarrow\pi^*)$ potential energy curves. The S_2 and T_1 potential energy profiles, on the other hand, run essentially parallel.

Electronic SOMEs calculated at the S_2 saddle point are shown in Table 5. Spin−orbit coupling between the $S_2(\pi\rightarrow\pi^*)$ and $T_1(\pi\rightarrow\pi^*)$ states is found to be small as may be expected for two states with similar electronic structures. Moreover, the significant energy gap combined with a lack of substantial geometric shifts yields negligible FC factors for a radiationless transition between these states. A participation of this channel

TABLE 5: Spin−Orbit Matrix Elements (cm^{-1}) Calculated at the TDDFT Optimized S_2 Geometry of Uracil Using the DFT/MRCI/TZVP Method for Generating the Wave Function

$\langle S_2\|\hat{H}_{SO,x}\|T_1\rangle$	−0.59
$\langle S_2\|\hat{H}_{SO,y}\|T_1\rangle$	−0.73
$\langle S_2\|\hat{H}_{SO,z}\|T_1\rangle$	−0.01
sum of squares	<1
$\langle S_2\|\hat{H}_{SO,x}\|T_2\rangle$	−18.98
$\langle S_2\|\hat{H}_{SO,y}\|T_2\rangle$	12.47
$\langle S_2\|\hat{H}_{SO,z}\|T_2\rangle$	0.83
sum of squares	516
$\langle S_2\|\hat{H}_{SO,x}\|T_3\rangle$	−3.43
$\langle S_2\|\hat{H}_{SO,y}\|T_3\rangle$	0.78
$\langle S_2\|\hat{H}_{SO,z}\|T_3\rangle$	0.12
sum of squares	12

TABLE 6: Rate Constants k_{ISC} (s^{-1}) for the (S_2 ⇝ T_2) and (S_2 ⇝ T_3) ISC Channels in Uracil Calculated at the DFT/MRCI/TZVP//DFT B3-LYP/TZVP Level[a]

channel	ΔE^{ad}	approximation	k_{ISC}
(S_2 ⇝ T_2)	11391	FC[b]	$\simeq 0.2 \times 10^{12}$
(S_2 ⇝ T_3)	5355	FC[c]	0.32×10^{9}
(S_2 ⇝ T_3)	5355	FC[c]+HT[d]	0.36×10^{9}

[a] ΔE^{ad} (cm^{-1}) denotes the adiabatic electronic energy difference. [b] Interval width of $\eta = 0.01$ cm^{-1} used. All vibrational modes were employed and 5 quanta per mode were allowed. An ISC rate of 0.16×10^{12} was obtained for an energy gap of 9000 cm^{-1}. The discrete summation over FC factors could not be carried out for an adiabatic energy difference as large as 11 391 cm^{-1}. [c] Interval width of $\eta = 0.01$ cm^{-1} used. All vibrational modes were employed and an unlimited number of quanta per mode were allowed. [d] Interval width of $\eta = 0.01$ cm^{-1} used. Derivative couplings for all vibrational modes were employed. The number of quanta per mode was limited to at most 1.

in the photophysics of uracil and its methylated derivatives can therefore be ruled out. Because of the admixture of n → π* character into the $S_2(\pi\rightarrow\pi^*)$ wave function, the coupling matrix element with the $T_2(n\rightarrow\pi^*)$ state is somewhat reduced at this geometry whereas the $\langle S_2|\hat{H}_{SO}|T_3\rangle$ matrix elements are significantly larger than typical $^1\pi \rightarrow \pi^*/^3\pi \rightarrow \pi^*$ SOMEs that are obtained, e.g., for the S_2 and T_1 pair of states. Despite the intersection of the two PEHs, the rate constant for the S_2 ⇝ T_3 is rather small (Table 6), even if HT-like vibronic spin−orbit coupling is invoked. Only the ISC rate for the S_2 ⇝ T_2 transition is found to be substantial. It is of similar magnitude to the rate for the S_1 ⇝ T_1 channel. The presence or absence of a true $S_2(\pi\rightarrow\pi^*)$ minimum will have only minor influence on the ISC rate. However, it will have large impact on the rates for the spin-allowed decay processes of the S_2 population via close-by conical intersections. As long as these concurrent processes take place on a much faster time scale, the spin-forbidden S_2 ⇝ T_2 transition cannot compete.

Summary and Conclusion

We have studied the properties of the isolated nucleo bases uracil, thymine, and 1-methylthymine in their ground and low-lying excited states. Particular emphasis has been placed on vibrational spectra in the $T_1(^3\pi\rightarrow\pi^*)$ and $S_1(^1n\rightarrow\pi^*)$ states, since these data can be used to identify the nature of the long-lived dark state that had been observed in these pyrimidine bases.[27,36−40] We find two indications in favor of the assignment of this state to the $T_1(^3\pi\rightarrow\pi^*)$ state. The experimentally observed lifetimes of the dark state are at least 1000 times longer than our computed time constants for the S_1 ⇝ T_1 decay. We thus conclude that the S_1 is not a likely candidate for the dark state. Comparison of our calculated difference infrared spectra for the S_0-T_1 and S_0-S_1 states with experimental data of Hare et al.[40] clearly shows that the time-resolved infrared spectrum, recorded by these authors, is due to vibrational excitation in the $T_1(^3\pi\rightarrow\pi^*)$ state.

How is the triplet state formed? It is agreed in the literature that most of the excited-state population that is initially generated in the $S_2(^1\pi\rightarrow\pi^*)$ state decays on a subpicosecond time scale to the electronic ground state, either by a direct route or via the intermediate $S_1(^1n\rightarrow\pi^*)$ state.[1−21] Nevertheless, substantial triplet quantum yields are found in aprotic solvents.[24,39] In the present work we have investigated several pathways for singlet−triplet intersystem crossing. In agreement with earlier proposals,[11,39−42] we find two fast ISC channels for the population of the $T_1(^3\pi\rightarrow\pi^*)$ state: (a) A nonradiative transition from the intermediate $S_1(^1n\rightarrow\pi^*)$ state directly to the T_1 state and (b) a transition from the initially populated $S_2(^1\pi\rightarrow\pi^*)$ state to $T_2(^3n\rightarrow\pi^*)$ followed by internal conversion to the T_1 state. In both cases, our calculations yield time constants for the singlet−triplet transition on the order of 10 ps. Due to the presence of the ultrafast S_2 ⇝ S_0 and S_2 ⇝ S_1 decay channels, the spin-forbidden S_2 ⇝ T_2 transition is not competitive, however. Our results therefore support the S_2 ⇝ S_1 ⇝ T_1 mechanism proposed by Hare et al.[11,39] where the intermediate S_1 state serves as a gateway for the triplet formation in uracil and its methylated derivatives. The strong solvent dependence of the triplet quantum yield[24,39] could be a consequence of the relative probabilities for the S_2 ⇝ S_0 and S_2 ⇝ S_1 decay processes following the initial $S_2 \leftarrow S_0$ excitation. To derive a complete picture of all competing decay processes of the photoexcited pyrimidine bases will require dynamical studies that include nonadiabatic and spin−orbit coupling on the same footing.

Acknowledgment. Financial support of this project by the Deutsche Forschungsgemeinschaft (DFG) through SFB 663 is gratefully acknowledged.

Supporting Information Available: Harmonic vibrational frequencies and Cartesian coordinates of all stationary points, simulated S_0-T_1 and S_0-S_1 difference spectra and the dependence of the computed ISC rates on technical parameters. This material is available free of charge via the Internet at http://pubs.acs.org.

References and Notes

(1) Crespo-Hernández, C. E.; Cohen, B.; Hare, P. M.; Kohler, B. *Chem. Rev.* **2004**, *104*, 1977–2019.
(2) Kang, H.; Lee, K. T.; Jung, B.; Ko, Y. J.; Kim, S. K. *J. Am. Chem. Soc.* **2002**, *124*, 12958–12959.
(3) Ullrich, S.; Schultz, T.; Zgierski, M. Z.; Stolow, A. *Phys. Chem. Chem. Phys.* **2004**, *6*, 2796–2801.
(4) Samoylova, E.; Lippert, H.; Ullrich, S.; Hertel, I. V.; Radloff, W.; Schultz, T. *J. Am. Chem. Soc.* **2005**, *127*, 1782–1786.
(5) Canuel, C.; Mons, M.; Piuzzi, F.; Tardivel, B.; Dimicoli, I.; Elhanine, M. *J. Chem. Phys.* **2005**, *122*, 074316-1−074316-6.
(6) Schneider, M.; Maksimenka, R.; Buback, F. J.; Kitsopoulis, T.; Lago, L. R.; Fisher, I. *Phys. Chem. Chem. Phys.* **2006**, *8*, 3017–3021.
(7) Peon, J.; Zewail, A. H. *Chem. Phys. Lett.* **2001**, *348*, 255–262.
(8) Pecourt, J.-M. L.; Peon, J.; Kohler, B. *J. Am. Chem. Soc.* **2001**, *123*, 10370–10378.
(9) Gustavsson, T.; Sharonov, A.; Markovitsi, D. *Chem. Phys. Lett.* **2002**, *351*, 195–200.
(10) Gustavsson, T.; Bányász, A.; Lazzarotto, E.; Markovitsi, D.; Scalmani, G.; Frisch, M.; Barone, V.; Improta, R. *J. Am. Chem. Soc.* **2006**, *128*, 607–619.
(11) Hare, P. M.; Crespo-Hernández, C. E.; Kohler, B. *Proc. Natl. Acad. Sci. U.S.A.* **2007**, *104*, 435–440.

(12) Matsika, S. *J. Phys. Chem. A* **2004**, *108*, 7584–7590.
(13) Tomić, K.; Tatchen, J.; Marian, C. M. *J. Phys. Chem. A* **2005**, *109*, 8410–8418.
(14) Zgierski, M. Z.; Patchkovskii, S.; Fujiwara, T.; Lim, E. C. *J. Phys. Chem. A.* **2005**, *109*, 9384–9387.
(15) Perun, S.; Sobolewski, A. L.; Domcke, W. *J. Phys. Chem. A* **2006**, *110*, 13238–13244.
(16) Merchán, M.; González-Luque, R.; Climent, T.; Serrano-Andrés, L.; Rodríguez, E.; Reguero, M.; Peláez, D. *J. Phys. Chem. B* **2006**, *110*, 26471–26476.
(17) Yoshikawa, A.; Matsika, S. *Chem. Phys.* **2008**, *347*, 393–404.
(18) Zechmann, G.; Barbatti, M. *J. Phys. Chem. A* **2008**, *112*, 8273–8279.
(19) Hudock, H. R.; Levine, B. G.; Thompson, A. L.; Satzger, H.; Townsend, D.; Gador, N.; Ullrich, S.; Stolow, A.; Martínez, T. J. *J. Phys. Chem. A* **2007**, *111*, 8500–8508.
(20) Nieber, H.; Doltsinis, N. L. *Chem. Phys.* **2008**, *347*, 405–412.
(21) Lan, Z.; Fabiano, E.; Thiel, W. *J. Phys. Chem. B* **2009**, *113*, 3548–3555.
(22) Cadet, J.; Vigny, P. *Bioorganic Photochemistry*; Wiley: New York, 1990; Vol. 1, pp 1−272.
(23) Douki, T.; Cadet, J. *Photochem. Photobiol. Sci.* **2003**, *2*, 433–436.
(24) Bishop, S. M.; Malone, M.; Philips, D.; Parker, A. W.; Symons, M. C. R. *J. Chem. Soc., Chem. Commun.* **1994**, 871–872.
(25) Marguet, S.; Markovitsi, D. *J. Am. Chem. Soc.* **2005**, *127*, 5780–5781.
(26) Schreier, W. J.; Schrader, T. E.; Koller, F. O.; Gilch, P.; C. E.; Crespo-Hernández, V. N. S.; Carell, T.; Zinth, W.; Kohler, B. *Science* **2007**, *315*, 625–629.
(27) Kwok, W.-M.; Ma, C.; Phillips, D. L. *J. Am. Chem. Soc.* **2008**, *130*, 5131–5139.
(28) Zhang, R. B.; Eriksson, L. A. *J. Phys. Chem. B* **2006**, *110*, 7556–7562.
(29) Boggio-Pasqua, M.; Groenhof, G.; Schaefer, L. V.; Grubmueller, H.; Robb, M. A. *J. Am. Chem. Soc.* **2007**, *129*, 10996–10997.
(30) Blancafort, L.; Migani, A. *J. Am. Chem. Soc.* **2007**, *129*, 14540–14541.
(31) Roca-Sanjuan, D.; Olaso-González, G.; González-Ramirez, I.; Serrano-Andrés, L.; Merchán, M. *J. Am. Chem. Soc.* **2008**, *130*, 10768–10779.
(32) Clark, L. B.; Peschel, G. G.; Tinoco, I., Jr. *J. Phys. Chem.* **1965**, *69*, 3615–3618.
(33) Abouaf, R.; Pommier, J.; Dunet, H. *Chem. Phys. Lett.* **2003**, *381*, 486–494.
(34) Brady, B. B.; Peteanu, L. A.; Levy, D. H. *Chem. Phys. Lett.* **1988**, *147*, 538–543.
(35) Mercier, Y.; Santoro, F.; Reguero, M.; Improta, R. *J. Phys. Chem. B* **2008**, *112*, 10769–10772.
(36) He, Y.; Wu, C.; Kong, W. *J. Phys. Chem. A* **2003**, *107*, 5143–5148.
(37) He, Y.; Wu, C.; Kong, W. *J. Phys. Chem. A* **2004**, *108*, 943–949.
(38) Busker, M.; Nispel, M.; Häber, T.; Kleinermanns, K.; Etinski, M.; Fleig, T. *Chem. Phys. Chem.* **2008**, *9*, 1570–1577.
(39) Hare, P. M.; Crespo-Hernández, C. E.; Kohler, B. *J. Phys. Chem. B* **2006**, *110*, 18641–18650.
(40) Hare, P. M.; Middleton, C. T.; Mertel, K. I.; Herbert, J. M.; Kohler, B. *Chem. Phys.* **2008**, *347*, 383–392.
(41) Climent, T.; González-Luque, R.; Merchán, M.; Serrano-Andrés, L. *Chem. Phys. Lett.* **2007**, *441*, 327–331.
(42) Serrano-Pérez, J. J.; González-Luque, R.; Merchán, M.; Serrano-Andrés, L. *J. Phys. Chem. B* **2007**, *111*, 11880–11883.
(43) Henry, B. R.; Siebrand, W. *J. Chem. Phys.* **1971**, *54*, 1072–1085.
(44) Christiansen, O.; Koch, H.; Jørgensen, P. *Chem. Phys. Lett.* **1995**, *243*, 409–418.
(45) Vahtras, O.; Almlöf, J.; Feyereisen, M. W. *Chem. Phys. Lett.* **1993**, *213*, 514–518.
(46) Hättig, C.; Weigend, F. *J. Chem. Phys.* **2000**, *113*, 5154–5161.
(47) Hättig, C. *J. Chem. Phys.* **2003**, *118*, 7751–7761.
(48) Köhn, A.; Hättig, C. *J. Chem. Phys.* **2003**, *119*, 5021–5036.
(49) Hättig, C.; Köhn, A. *J. Chem. Phys.* **2002**, *117*, 6939–6951.
(50) Bauernschmitt, R.; Ahlrichs, R. *Chem. Phys. Lett.* **1996**, *256*, 454–464.
(51) Becke, A. D. *J. Chem. Phys.* **1993**, *98*, 5648–5652.
(52) Ahlrichs, R.; et al. *TURBOMOLE (Vers. 5.7)*; Universität Karlsruhe: Germany, 2004.
(53) Neugebauer, J.; Reiher, M.; Kind, C.; Hess, B. A. *J. Comput. Chem.* **2002**, *23*, 895–910.
(54) Grimme, S.; Waletzke, M. *J. Chem. Phys.* **1999**, *111*, 5645–5655.
(55) Becke, A. D. *J. Chem. Phys.* **1993**, *98*, 1372–1377.
(56) Lee, C.; Yang, W.; Parr, R. G. *Phys. Rev. B* **1988**, *37*, 785–789.
(57) Dunning, T. H. *J. Chem. Phys.* **1989**, *90*, 1007–1023.
(58) Kendall, R. A.; Dunning, T. H. J.; Harrison, R. J. *J. Chem. Phys.* **1992**, *96*, 6796–6806.
(59) Schäfer, A.; Huber, C.; Ahlrichs, R. *J. Chem. Phys.* **1994**, *100*, 5829–5835.
(60) Weigend, F.; Köhn, A.; Hättig, C. *J. Chem. Phys.* **2002**, *116*, 3175–3183.
(61) Eichkorn, K.; Weigend, F.; Treutler, O.; Ahlrichs, R. *Theor. Chem. Acc.* **1997**, *97*, 119–124.
(62) Kleinschmidt, M.; Tatchen, J.; Marian, C. M. *J. Comput. Chem.* **2002**, *23*, 824–833.
(63) Schimmelpfennig, B. *AMFI*; Stockholm University: Sweden, 1996.
(64) Hess, B. A.; Marian, C. M.; Wahlgren, U.; Gropen, O. *Chem. Phys. Lett.* **1996**, *251*, 365–371.
(65) Tatchen, J.; Marian, C. M. *Chem. Phys. Lett.* **1999**, *313*, 351–357.
(66) Danovich, D.; Marian, C. M.; Neuheuser, T.; Peyerimhoff, S. D.; Shaik, S. *J. Phys. Chem. A* **1998**, *102*, 5923–5936.
(67) Tatchen, J.; Gilka, N.; Marian, C. M. *Phys. Chem. Chem. Phys.* **2007**, *9*, 5209–5221.
(68) Salzmann, S.; Tatchen, J.; Marian, C. M. *J. Photochem. Photobio. A* **2008**, *198*, 221–231.
(69) Fleig, T.; Knecht, S.; Hättig, C. *J. Phys. Chem. A* **2007**, *111*, 5482–5491.
(70) Steward, R. F.; Jensen, L. H. *Acta Chrystallogr.* **1967**, *23*, 1102–1105.
(71) Vogt, N.; Khaikin, L. S.; Grikina, O. E.; Rykov, A. N.; Vogt, J. *J. Phys. Chem. A* **2008**, *112*, 7662–7670.
(72) Colarusso, P.; Zhang, K.; Guo, B.; Bernath, P. F. *Chem. Phys. Lett.* **1997**, *269*, 39–48.
(73) Petke, J. D.; Maggiora, G. M.; Christoffersen, R. E. *J. Phys. Chem.* **1992**, *96*, 6992–7001.
(74) Lorentzon, J.; Fülscher, M. P.; Roos, B. O. *J. Am. Chem. Soc.* **1995**, *117*, 9265–9273.
(75) Broo, A.; Holmén, A. *J. Phys. Chem.* **1997**, *101*, 3589–3600.
(76) Marian, C. M.; Schneider, F.; Kleinschmidt, M.; Tatchen, J. *Eur. Phys. J. D* **2002**, *20*, 357–367.
(77) Epifanovsky, E.; Kowalski, K.; Fan, P.-D.; Valiev, M.; Matsika, S.; Krylov, A. I. *J. Phys. Chem. A* **2008**, *112*, 9983–9992.
(78) Schreiber, M.; Silva-Junior, M.; Sauer, S. P. A.; Thiel, W. *J. Chem. Phys.* **2008**, *128*, 134110-1–134110-25.
(79) Silva-Junior, M. R.; Schreiber, M.; Sauer, S. P. A.; Thiel, W. *J. Chem. Phys.* **2008**, *129*, 104103-1–104103-14.
(80) Etinski, M.; Fleig, T.; Marian, C. M. Manuscript in preparation.
(81) Nguyen, M. T.; Zhang, R.; Nam, P.-C.; Ceulemans, A. *J. Phys. Chem. A* **2004**, *108*, 6554–6561.

JP902944A